The electronic and magnetic structure of Fe-based bulk amorphous metals: An ab-initio approach

Yang Wang[1], Mike Widom[2], Don Nicholson[3], Marek Mihalkovic[2], and Siddartha Naidu[2]
[1]Pittsburgh Supercomputing Center, Carnegie Mellon University, Pittsburgh, PA 15213
[2]Department of Physics, Carnegie Mellon University, Pittsburgh, PA 15213
[3]Computer Science and Mathematics Division, Oak Ridge National Laboratory, Oak Ridge, TN 37831

ABSTRACT

We applied the locally self-consistent multiple scattering (LSMS) method to the study Fe-based bulk amorphous metals. The LSMS method is an order-N approach to the electronic structure calculation for solid state materials based on density functional theory and local density approximation. Using LSMS method, we performed electronic structure calculations for the supercell samples generated by ab-initio molecular dynamics simulation. The equilibrium atomic volume and the bulk modulus are calculated based on the energy versus volume curve. The magnetic moment distribution in the samples is determined for both collinear and noncollinear cases. A comparison with the experimental results is also made.

INTODUCTION

Amorphous metals prepared by rapid quenching technique from the liquid state were first reported in 1960 [1]. Also known as metallic glasses, they differ from ordinary metals in that their constituent atoms are not arranged on a crystalline lattice. Because of this, they exhibit unique combination of physical properties and have attracted much attention from both industrial and academic institutions [2,3]. Nevertheless, until recently, they have largely been manufactured in the form of thin ribbons usually less than 1mm in thickness, because fast cooling rates (~ 10^6 ˚K/sec) are required for retaining the metastable amorphous phase. And as a result, they have not attained an important role of industrial applicability.
The first reported bulk amorphous metals were Pd-based alloys developed in the early 1980s [4,5]. Of these, Pd-Ni-P alloys were prepared with thicknesses up to 1 cm [5] which demonstrated that the 1mm thickness limits can be surmounted. But they did not draw sufficient interests from industry due to the high cost of palladium. The real breakthrough came during the period from 1988 to 1990 when Inoue et al. [6-8] discovered multicomponent liquid alloys with very deep eutectics capable of freezing to a glassy state of several cm thick by conventional cooling methods. This indeed proved to be a turning point in opening up a new field of research. Beginning with Mg- [6], Ln- [7] and Zr- [8] based quaternary alloys, Inoue extended bulk amorphous metal formation to Fe-, Ni- and other alloy families. (See reference [9] for a historical summary on Inoue's discovery of bulk amorphous metals.) Johnson's group developed Zr-Ti-based and other sizable amorphous metals [10-12]. Poon et al. proposed Zr-B and Mo-C backbone structure model in Fe-based bulk amorphous metals, and recently produced Fe-Mn-based bulk glass samples [13].
Bulk amorphous metals exhibit low volume shrinkage, high mechanical strength and hardness, low surface roughness, and possibly high resistance to corrosions. Due to these unique physical

properties, they have been proposed for a range of potential applications in sporting goods materials, medical and dental implants, machining tools, coatings, and more. Especially, Fe-based soft magnetic bulk amorphous metals that show high saturation magnetization and high permeability can be used as magnetic core materials in transformers and electrical motors. Recently, a number of so called amorphous steel alloys have been found [13]. These are nonmagnetic Fe-based glassy alloys with Curie temperatures below −100 ˚C and have potential nonmagnetic structural applications.

As a first step towards understanding and prediction of the glass formability and the magnetic structure of Fe-based alloys, we carried out theoretical investigation of the alloys using atomic scale simulation techniques. In the following sections, we will first provide a description of our theoretical approach. We will show the results from the electronic structure calculations and discuss the comparison with experiment. And finally, we will arrive to our conclusions.

THEORETICAL APPROACH

Theoretical approach to alloys usually starts with alloy structure simulation by constructing a unit cell, consisting of the constituent atoms in a predetermined proportion, to mimic the atomic composition and arrangement in the real alloy. Unlike ordinary alloys in crystalline state, however, an alloy in amorphous phase does not have an underline lattice. This requires that, after being randomly placed in the unit cell, the atoms be relaxed from their location in space by a quenching process starting from a high temperature to a low temperature. In our approach, the atomic movement during the quenching process is treated classically while the force field that drives the atomic displacement is determined quantum mechanically. The entire simulation is carried out using the Vienna *Ab-initio* Simulation Program (VASP) [14], a software package capable of performing *ab-initio* molecular dynamics simulations. The pair distribution function of the unit cell sample in its final structure can be directly calculated and compared with experiment. For a detailed description of our work on structural simulation for bulk amorphous metals, we refer to the paper by Widom et al. [15] in this proceeding.

Given a unit cell sample that resembles the amorphous structure of an alloy, we apply the locally self-consistent multiple scattering (LSMS) method [16] to calculate the electronic and magnetic structures of the alloy. The LSMS method is an order-N approach to the *ab-initio* electronic structure calculation. By order-N, we mean that the computational effort of the LSMS method scales linearly with respect to the number of atoms in the unit cell, rather than cubically like most other *ab-initio* methods. Because it is based on multiple scattering theory, the LSMS method allows an approximate calculation of the Green function associated with the Kohn-Sham's one-electron Schrödinger equation [17] derived from the density functional theory [18] with local spin density approximation [19]. The electron density and the magnetic moment density in the vicinity of the *i*th atom are taken from the imaginary part of the Green function as follows:

$$\begin{aligned} \rho_i(\boldsymbol{r}) &= -\frac{1}{\pi}\,\mathrm{Im}\,Tr\int_{-\infty}^{\varepsilon_F} d\varepsilon \underline{G}_i(\boldsymbol{r},\boldsymbol{r};\varepsilon), \\ \boldsymbol{m}_i(\boldsymbol{r}) &= -\frac{1}{\pi}\,\mathrm{Im}\,Tr\int_{-\infty}^{\varepsilon_F} d\varepsilon \left[\underline{G}_i(\boldsymbol{r},\boldsymbol{r};\varepsilon)\cdot\underline{\boldsymbol{\sigma}}\right], \end{aligned} \tag{1}$$

where the Green function $\underline{G}_i(\boldsymbol{r},\boldsymbol{r};\varepsilon)$ is a 2 × 2 matrix in the spinor space and is calculated in the vicinity of atom *i* with assumption that the atom only sees its neighboring atoms within a local

interaction zone. Each component of the vector $\underline{\boldsymbol{\sigma}}$ is a Pauli matrix, and ε_F is the Fermi energy. The energy integration usually takes place along an energy contour in the upper half complex plane. The density of states associated with atom *i* for spin up (+) or spin down (−) state along an arbitrary direction $\boldsymbol{A}$ is given by

$$\rho_i^{\pm}(\varepsilon) = -\frac{1}{2\pi}\,\mathrm{Im}\,Tr\int_{\Omega_i} d^3r\left[\underline{G}_i(\boldsymbol{r},\boldsymbol{r};\varepsilon)\cdot(\underline{1}\pm\boldsymbol{\sigma}\cdot\boldsymbol{A})\right], \qquad (2)$$

where $\underline{1}$ is a 2 × 2 identity matrix and the volume integration is carried out over Ω_i, the atomic cell associated with atom *i*. For ferromagnetic states, the Green function matrix is diagonal in the frame of references that the *z*-axis is along the magnetization direction, and the computational procedure can be much simplified by carrying out the spin-polarized calculation, for which the Green function for spin up and spin down states is decoupled and is calculated separately. For non-collinear magnetic states, the Green function matrix is non-diagonal and its calculation, also known as spin-canted calculation, usually takes four times longer than the spin-polarized calculation. To find the ground state electronic and magnetic structure of a non-collinear magnetic alloy system, we start with a random distribution of the local moments on each atom and allow the moments under the influence of a local effective magnetic field to rotate. The local effective magnetic field is the summation of the local exchange field resulting from the local spin density approximation and the local transverse constraining field [20] which is necessary for maintaining the orientation of the local moments unchanged between each time step while we are searching for the electronic ground state associated with the given magnetic moment configuration. This spin dynamics algorithm is made possible by the fact that the fast electronic motion (~ 10^{-15} sec) and the slow moment rotation motion (~ 10^{-13} sec) can be treated separately. The spin dynamics simulation ends when the final ground state is reached. In the final ground state, the constraining field acting on each atom is zero and the local exchange field is collinear with the local magnetization orientation [20].

RESULTS

We investigated two Fe-based bulk amorphous metal systems: $Fe_{0.48}Mn_{0.20}Zr_{0.10}B_{0.22}$ and $Fe_{0.50}Mn_{0.15}Mo_{0.15}C_{0.15}B_{0.05}$. Both systems are Fe-rich and contain manganese, refractory metals (Zr and Mo) and metalloids (B). It has been proposed in "backbone model" by Poon et al. [13] that Zr-B and Mo-C constitute the strong backbone structures in these two Fe-based bulk amorphous metals. The backbone structure is a structure-reinforced network formed by tightly bound components in the under-cooled liquid and is believed to be one of few essential factors contributing to the high formability of bulk amorphous metals. It is also known that the Mn as well as the refractory metals is very effective in suppressing ferromagnetism in Fe-based amorphous alloys. In our effort to searching for amorphous steel alloys for nonmagnetic structural applications, these two alloy systems are obviously the potential candidate.
A set of quenched structural samples of $Fe_{0.48}Mn_{0.20}Zr_{0.10}B_{0.22}$ and $Fe_{0.50}Mn_{0.15}Mo_{0.15}C_{0.15}B_{0.05}$ are generated using VASP [15]. These samples are tetragonal shaped unit cell that contains 100 atoms with desired composition. Based on numerous experimental evidences, it has been suggested that some Fe-base amorphous alloys exist in a non-collinear magnetic state. This non-collinear magnetic state appears to persist in applied fields well in excess of the saturation field of the alloys. We applied LSMS method to the electronic and magnetic structure calculations for both ferromagnetic and non-collinear magnetic states. Specifically, the spin-polarized

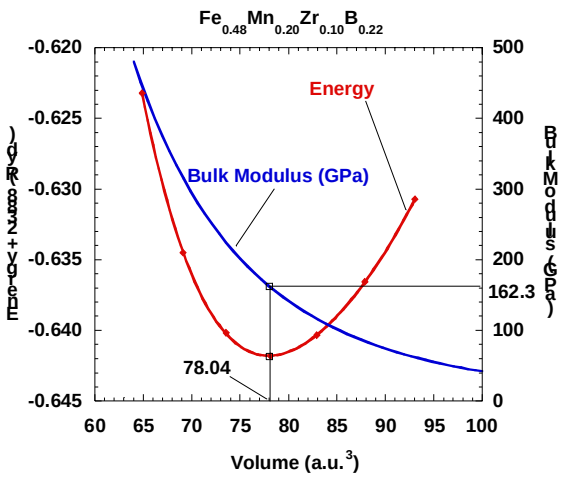

Figure 1(a). $Fe_{0.48}Mn_{0.20}Zr_{0.10}B_{0.22}$: Total energy (in Ryd) and bulk modulus (in GPa) per atom versus averaged atomic volume (in atomic units).

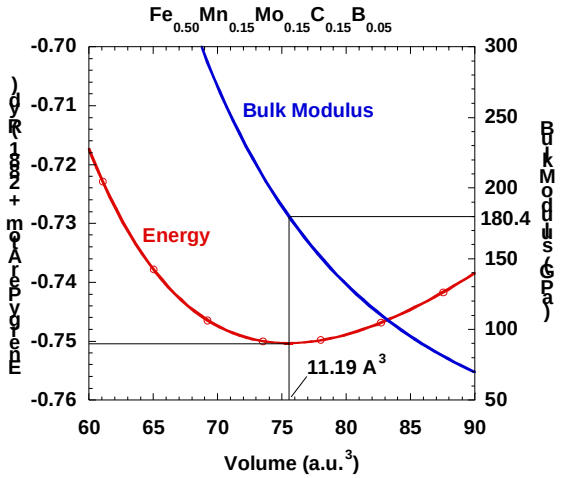

Figure 1(b). $Fe_{0.50}Mn_{0.15}Mo_{0.15}C_{0.15}B_{0.05}$: Total energy (in Ryd) and bulk modulus (in GPa) per atom versus averaged atomic volume (in atomic units).

calculations are carried out for the ferromagnetic states of each unit cell sample with various volumes, which are either compressed or expanded from the unit cell generated by VASP. The total energy per atom and the bulk modulus per atom versus the averaged atomic volume are plotted in Fig. 1(a) for a $Fe_{0.48}Mn_{0.20}Zr_{0.10}B_{0.22}$ sample and in Fig. 1(b) for a $Fe_{0.50}Mn_{0.15}Mo_{0.15}C_{0.15}B_{0.05}$ sample. At the ground state, where the total energy is at the minimum, the atomic volume and bulk modulus are found to be 11.56 $Å^3$ and 162.3 GPa, respectively, for the FeMnZrB sample and 11.2 $Å^3$ and 180.4 GPa, respectively, for the FeMnMoCB sample. An estimate from experiment [21] gives 11.6 $Å^3$ for the atomic volume for FeMnZrB with similar composition. For $Fe_{0.50}Mn_{0.15}Mo_{0.15}C_{0.15}B_{0.05}$, the experimental measurement [21] gives 10.9 $Å^3$ for the atomic volume and 190 GPa for the bulk modulus. The magnetic moment per atom versus the averaged atomic volume is plotted in Fig 2(a) and Fig 2(b). At the experimental volume, we also performed spin-canted calculation together with spin dynamics simulation to search for the ground state magnetic moment configuration. The magnetic moment per atom value of the non-collinear state is $0.25\mu_B$ for $Fe_{0.48}Mn_{0.20}Zr_{0.10}B_{0.22}$ and $0.21\mu_B$ for $Fe_{0.50}Mn_{0.15}Mo_{0.15}C_{0.15}B_{0.05}$. These values are indicated by a solid circle in Fig 2(a) and Fig 2(b). We have also performed the calculation on another $Fe_{0.48}Mn_{0.20}Zr_{0.10}B_{0.22}$ sample which is generated by a different quenching process by VASP simulation. The magnetic moment of the non-collinear magnetic state is found to be $0.51\mu_B$ per atom. For comparison, we note that the experimental measurement [21] on a FeMnMoCB sample gives $0.23\mu_B$ per atom, and the measurement on a $(Fe_{0.69}Mn_{0.26}Cr_{0.05})_{0.68}Zr_{0.04}Nb_{0.04}B_{0.24}$ sample gives $0.56\mu_B$ per atom.

DISCUSSIONS AND CONCLUSIONS

In the previous section, we present the calculated results for two Fe-based amorphous samples: $Fe_{0.48}Mn_{0.20}Zr_{0.10}B_{0.22}$ and $Fe_{0.50}Mn_{0.15}Mo_{0.15}C_{0.15}B_{0.05}$. Comparison is also made with available

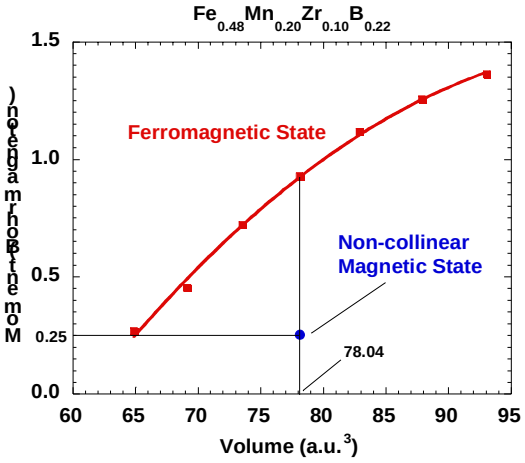

Figure 2(a). $Fe_{0.48}Mn_{0.20}Zr_{0.10}B_{0.22}$: Magnetic moment (in Bohr magneton) per atom versus averaged atomic volume (in atomic units).

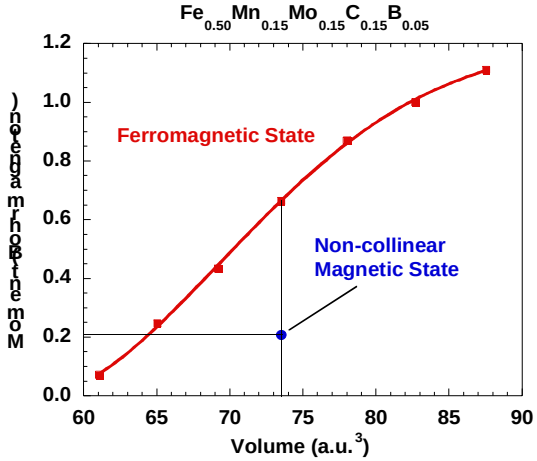

Figure 2(b). $Fe_{0.50}Mn_{0.15}Mo_{0.15}C_{0.15}B_{0.05}$: Magnetic moment (in Bohr magneton) per atom versus averaged atomic volume (in atomic units).

experimental values for the bulk amorphous metals with similar compositions. The overall agreement between the calculation and the experiment is considered to be excellent.

In our approach, we performed energy versus volume calculation for ferromagnetic states rather than non-collinear magnetic states. We note that both spin-polarized and spin-canted calculations give essentially the same energy curve, since the non-collinear magnetic state makes less than 10^{-3} Ryd energy difference from the ferromagnetic state. This allows us to save a lot of computer time for the calculation of the energy versus volume curve. However, as we observed from the calculation, the magnetic moment of the non-collinear magnetic state is much less than the ferromagnetic moment. This indicates that the suppression of overall magnetic moment in these two types of Fe-based amorphous metals is essentially driven by the existence of the non-collinear magnetic state. Finally, we note that, while they are much less than the ferromagnetic moment value, the calculated non-collinear moment values for two different FeMnZrB samples are quite different. This can be attributed to the fact that the moment orientation and magnitude of each atom is largely determined by the local chemical environment. Note that the unit cell size in our calculation is 100 atoms, due to the computational limit of VASP. When two different samples are generated, large moment variance can be observed because of the sample size effect. We are hoping to achieve better statistics to improve our spin dynamics calculation by going beyond 100 atoms per unit cell limit. One possible approach to this can be artificially assembling together multiple 100-atom unit cell samples to make a larger unit cell sample, which can contain hundreds or thousands of atoms.

ACKNOWLEDGMENTS

The authors thank their colleagues J. Poon, T. Egami, D. Louca, and G. Shiflet for helpful discussions. The research is supported by DARPA/ONR Grant N00014-01-1-0961. The VASP and LSMS calculations were performed at Pittsburgh Supercomputing Center.

REFERENCES

1. W. Klement, R.H. Willens, P. Duwez, *Nature* **187**, 869 (1960).
2. See articles in *Amorphous Metallic Alloys*, edited by F.E. Luborsky, (Butterworths, London, 1983).
3. R.W. Cahn, in *Glasses and Amorphous Materials*, edited by J. Zarzycki, (Mater. Sci. Tech. **9**, VCH Press, Weinheim, 1991) pp. 493-548.
4. H.W. Kui, A.L. Greer, and Turnbull, *Appl. Phys. Lett.* **45**, 615 (1984).
5. A.J. Drehman and A.L. Greer, *Acta. Metall.* **32**, 323 (1984).
6. A. Inoue, K. Ohtera, K. Kita, T. Masumoto, *Jpn. J. Appl. Phys.* **27**, L2248 (1988).
7. A. Inoue, T. Zhang, T. Masumoto, *Mater. Trans. JIM* **30**, 965 (1989).
8. A. Inoue, T. Zhang, T. Masumoto, *Mater. Trans. JIM* **31**, 148 (1990).
9. A. Inoue, *Mater. Sci. Eng.* **A304-306**, 1 (2001).
10. X.H. Lin and W.L. Johnson, *J. Appl. Phys.* **78**, 6514 (1995).
11. C.C. Hays, C. P. Kim, and W.L. Johnson, *Appl. Phys. Lett.* **75**, 1089 (1999).
12. C.C. Hays, J. Schroers, U. Geyer, S. Bossuyt, N. Stein, and W.L. Johnson, *Mater. Sci. Forum* **343**, 103 (2000).
13. S.J. Poon, G.J. Shiflet, F.Q. Guo, and V. Ponnambalam (*to be published*).
14. http://cms.mpi.univie.ac.at/vasp/vasp/vasp.html.
15. M. Widom, M. Mihalkovic, S. Naidu, D.M.C. Nicholson, and Y. Wang (to be published in MRS proceeding).
16. Y. Wang, G.M. Stocks, W.A. Shelton, D.M.C. Nicholson, W.M. Temmerman, and Z. Szotek, *Phys. Rev. Lett.* **75**, 2867 (1995).
17. W. Kohn and L.J. Sham, *Phys. Rev. A* **140**, 1133 (1965).
18. P.C. Hohenberg and W. Kohn, *Phys. Rev. B* **136**, 864 (1964).
19. U. von Barth and L. Hedin, *J. Phys. C.* **5**, 1629 (1972).
20. G.M. Stocks, B. Ujfalussy, X. Wang, D.M.C. Nicholson, W.A. Shelton, Y. Wang, A. Canning, and B.L. Gyorffy, *Phil. Mag. B*, **78**, 665 (1998).
21. J. Poon, *private communications*.